

AD-A255 897



Temperature Measurements with Micrometer Spatial Resolution

Prepared by

F. IZAGUIRRE and G. F. HAWKINS
Technology Operations

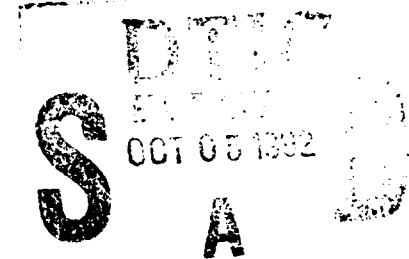
and

G. CSANKY
Electronics and Sensors Division

24 July 1992

Prepared for

SPACE AND MISSILE SYSTEMS CENTER
AIR FORCE MATERIEL COMMAND
Los Angeles Air Force Base
P. O. Box 92960
Los Angeles, CA 90009-2960



Engineering and Technology Group

THE AEROSPACE CORPORATION
El Segundo, California

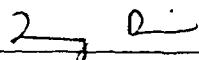
92-26371
208

TI 0 2 01 84

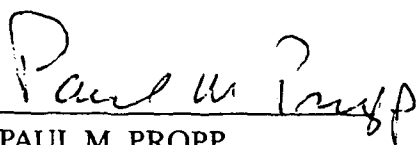
This report was submitted by The Aerospace Corporation, El Segundo, CA 90245-4691, under Contract No. F04701-88-C-0089 with the Space Systems Division, P.O. Box 92960-4691, Los Angeles, CA 90009-2960. It was reviewed and approved for The Aerospace Corporation by R. W. Fillers, Principal Director, Mechanics and Materials Technology Center; and J. M. Strauss, Principal Director, Communications Systems Subdivision. Paul M. Propp was the project officer for the Mission-Oriented Investigation and Experimentation program.

This report has been reviewed by the Public Affairs Office (PAS) and is releasable to the National Technical Information Service (NTIS). At NTIS, it will be available to the general public, including foreign nationals.

This technical report has been reviewed and is approved for publication. Publication of this report does not constitute Air Force approval of the report's findings or conclusions. It is published only for the exchange and stimulation of ideas.



QUANG BUI, Lt., USAF
MOIE Program Manager



PAUL M. PROPP
Wright Laboratory West Coast Office

UNCLASSIFIED

SECURITY CLASSIFICATION OF THIS PAGE

REPORT DOCUMENTATION PAGE				
1a. REPORT SECURITY CLASSIFICATION Unclassified		1b. RESTRICTIVE MARKINGS		
2a. SECURITY CLASSIFICATION AUTHORITY		3. DISTRIBUTION/AVAILABILITY OF REPORT Approved for public release; distribution unlimited		
2b. DECLASSIFICATION/DOWNGRADING SCHEDULE				
4. PERFORMING ORGANIZATION REPORT NUMBER(S) TR-0090(5938-08)-1		5. MONITORING ORGANIZATION REPORT NUMBER(S) SMC-TR-92-40		
6a. NAME OF PERFORMING ORGANIZATION The Aerospace Corporation Technology Operations	6b. OFFICE SYMBOL <i>(If applicable)</i>	7a. NAME OF MONITORING ORGANIZATION Space and Missile Systems Center		
6c. ADDRESS <i>(City, State, and ZIP Code)</i> El Segundo, CA 90245-4691		7b. ADDRESS <i>(City, State, and ZIP Code)</i> Los Angeles Air Force Base Los Angeles, CA 90009-2960		
8a. NAME OF FUNDING/SPONSORING ORGANIZATION	8b. OFFICE SYMBOL <i>(If applicable)</i>	9. PROCUREMENT INSTRUMENT IDENTIFICATION NUMBER F04701-88-C-0089		
8c. ADDRESS <i>(City, State, and ZIP Code)</i>		10. SOURCE OF FUNDING NUMBERS		
		PROGRAM ELEMENT NO.	PROJECT NO.	TASK NO.
		WORK UNIT ACCESSION NO.		
11. TITLE <i>(Include Security Classification)</i> Temperature Measurements with Micrometer Spatial Resolution				
12. PERSONAL AUTHOR(S) Izaguirre, Francisco; Csanky, Geza; and Hawkins, Gary F.				
13a. TYPE OF REPORT	13b. TIME COVERED FROM _____ TO _____	14. DATE OF REPORT <i>(Year, Month, Day)</i> 1992 July 24	15. PAGE COUNT 24	
16. SUPPLEMENTARY NOTATION				
17. COSATI CODES			18. SUBJECT TERMS <i>(Continue on reverse if necessary and identify by block number)</i> Fluorescence Junction temperature Semiconductor Thermometry	
FIELD	GROUP	SUB-GROUP		
19. ABSTRACT <i>(Continue on reverse if necessary and identify by block number)</i> A novel technique has been developed to measure temperatures with a spatial resolution less than 10 μm. This method uses the temperature-sensitive time decay fluorescence of a phosphor as a surface sensor. The spatial resolution is obtained by using an electron beam to excite individual phosphor grains deposited on the surface of interest. The phosphor selected for its dynamic range and chemical stability is the inorganic compound magnesium fluorogermanate activated with manganese. The time decay constant of its fluorescence decreases monotonically with temperature between -200 to 450°C. This method was verified on a cross-sectioned Zener diode. A description of the technique and a temperature map of the sectioned area of an operating diode are presented.				
20. DISTRIBUTION/AVAILABILITY OF ABSTRACT <input checked="" type="checkbox"/> UNCLASSIFIED/UNLIMITED <input type="checkbox"/> SAME AS RPT. <input type="checkbox"/> DTIC USERS		21. ABSTRACT SECURITY CLASSIFICATION Unclassified		
22a. NAME OF RESPONSIBLE INDIVIDUAL		22b. TELEPHONE <i>(Include Area Code)</i>	22c. OFFICE SYMBOL	

PREFACE

The authors express their appreciation to C. T. Hoskinson of The Aerospace Corporation for his support of this project.

Approved For	
NTIS	J
DTIC	
Unannounced	
Justification	
By	
Date	
DTIC	
A-1	

DTIC QUALITY INSPECTED 1

CONTENTS

PREFACE	1
I. INTRODUCTION	7
II. METHOD	9
A. Phosphor-Grain Thermometry	9
B. Sample Preparation	9
C. Experimental Setup	11
D. Procedure	13
III. RESULTS AND DISCUSSION	17
A. Thermal Characteristics of Zener Diodes	17
B. Experimental Uncertainty	18
IV. CONCLUSIONS	21
REFERENCES	23

FIGURES

1.	Block Diagram of Experimental Setup and Sketch of Sample Assembly	10
2.	Photomicrograph of Sectioned Zener Diode with Phosphor Grains	11
3.	Typical Luminescence Curve Obtained from a MFGe:Mn Phosphor Grain	13
4.	Time Decay vs Temperature Calibration Curve for a MFGe:Mn Phosphor Grain	14
5.	Thermal Map of Sectioned 22-V Zener Diode	15

TABLES

1.	Photon-Counter Gate Settings	12
2.	Total Thermal Resistance, Temperature Rise, and Junction Temperature for Various Segments of Zener Diode	18

I. INTRODUCTION

In many cases it is desirable to measure the surface temperature of a material using a technique that has a spatial resolution of less than 10 μm . For example, the measurements that can be used to ascertain the thermal profile of electronic components. All semiconductor devices have a finite life expectancy, and these profiles are required to calculate the life expectancy of the components. The main failure mode of these devices is thermally activated, and life expectancy can be verified in a relatively short time if a device is operated at a higher than its maximum operating temperature, provided that the failure mode of the device at elevated temperatures is the same as it is at normal operating temperatures. With this provision, the reliability of a semiconductor device can be predicted if the relationship between the junction temperature T_J of the thermal activation process and its mean time to failure is known. Temperature measurements can also be used to study the heat flow in high power devices such as laser diodes. The temperature profiles can be compared to the results of finite-element analysis codes to verify both the validity of the code input parameters and the life expectancy and performance of the parts.

Few techniques have been developed that yield thermal profiles with a spatial resolution better than 10 μm . This resolution is required to accurately determine the temperature profiles of many small components. The highest resolution technique was developed by Williams and Wickramasinghe¹ and uses a modified version of the equipment developed for the scanning tunneling microscope (STM). Another technique developed by Kolodner and Tyson² optically images a phosphor film deposited on the surface of interest and uses image processing techniques to measure luminescence intensity and determine the temperature profile. The technique we describe in this report complements work of Kolodner and Tyson by extending its capability to the spatial resolutions obtained by scanning electron microscopes (SEMs). Since this technique is performed in an SEM, it does not have the 100-nm resolution of the STM technique, but the basic equipment is more readily available, and it can be performed when extreme resolution is not required.

The method described here uses the temperature-sensitive time decay fluorescence of a phosphor as a surface sensor. The phosphor selected for its dynamic range and chemical stability is magnesium fluorogermanate activated with manganese. The phosphor grains are suspended in a diluted adhesive solution and deposited on the surface of interest. The spatial resolution is obtained by exciting individual phosphor grains that have diameters less than 10 μm with an electron beam. This method has been applied to measure the temperature profile of a 1N5251 axial-lead, plastic encapsulated, 500-mW, 22-V Zener diode under operation.

II. METHOD

A. PHOSPHOR-GRAIN THERMOMETRY

This method uses a phosphor as a surface temperature sensor.³ The use of a phosphor for this purpose is appropriate since the phosphor can be brought into good thermal contact with the surface; it does not alter appreciably the surface temperature of the device; and in powder form may have small grain size that offers the required spatial resolution. Additionally, most phosphors are electrical insulators and, therefore, do not alter the electrical properties of the surface on which they are placed. An electron beam was chosen to excite the phosphor because it can be focused to a few angstroms in diameter and individual grains can be independently excited.

The phosphor selected for our experiments consists of magnesium fluorogermanate activated with tetravalent manganese [$\text{Mg}_4(\text{F})\text{GeO}_6:\text{Mn}$]. The time decay fluorescence of this phosphor decreases monotonically and almost linearly with temperature over the range of -200 to $+450^\circ\text{C}$. Its emission is in the deep red (~ 658 nm), and its fluorescence versus time curve is nearly exponential. This phosphor has been used for determining temperature to an accuracy of $\pm 2^\circ\text{C}$ without any special calibration, provided that a large enough amount of material is used.⁴ This report describes a technique where individual grains with diameters of less than $10\ \mu\text{m}$ were excited with the electron beam from a scanning electron microscope (SEM).

B. SAMPLE PREPARATION

A 1N5251 22-V Zener diode was polished lengthwise to expose its cross section. After polishing, the diode maintained its reverse characteristics, and only minor degradation could be observed on a curve tracer. As shown in Fig. 1, the sectioned diode was mounted in a groove of a 1-in.-diameter copper disk and held in place with GE 7031 insulating varnish adhesive. A cartridge heater was embedded in the copper disk and fastened with the same adhesive. This adhesive is both a good heat conductor and an electrical insulator. A thermocouple, secured to the copper disk with a screw, continuously monitored the temperature of the copper block.

The phosphor was suspended in a diluted silicate adhesive solution. A drop of this solution was deposited over the exposed silicon area. Excess solution was removed by capillary action, by bringing a corner of a tissue paper in contact with the solution. In this manner, as measured with a profilometer, adhesive thin films with thicknesses of less than 300 nm were obtained. This film thickness is transparent in SEM micrographs. The adhesive used is a water-based silicate with excellent thermal conductivity. Additionally, it is transparent in the visible. It is stable in the temperature range compatible with that of the phosphor and remains flexible through the entire range. This reduces thermal stresses between the sample, the substrate, and the phosphor. The disk assembly was held in the SEM's specimen holder with three stainless-steel screws that terminated at a point. This minimized heat losses due to thermal conduction. The completed disk assembly was placed into the specimen chamber of the SEM. A micrograph of the Zener diode with the phosphor grains fastened to the silicon substrate is shown in Fig. 2.

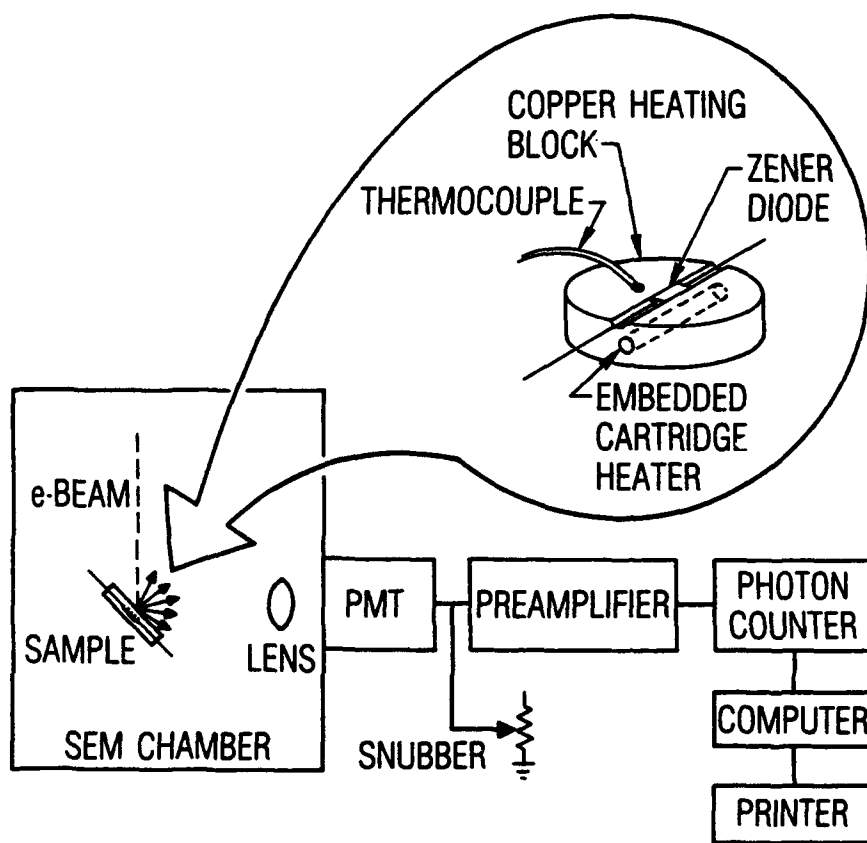


Figure 1. Block Diagram of Experimental Setup and Sketch of Sample Assembly

C. EXPERIMENTAL SETUP

Figure 1 also contains a block diagram of the experimental setup. The SEM was operated at 20 kV with a filament current of about 100 μ A. The SEM column was equipped with a beam blanking attachment that generated a short electron-beam pulse. This pulse, in turn, excited the phosphor. A port on the specimen chamber was fitted with a photomultiplier tube (PMT). A lens located in front of the PMT focused the emitted photons onto the tube's photocathode. The output of the PMT was amplified and monitored with a photon counter.



Figure 2. Photomicrograph of Sectioned Zener Diode with Phosphor Grains

During measurement, a single grain was selected from the SEM's image. The magnification was then increased until only the selected grain was being scanned by the SEM's electron beam. In this manner only one grain was excited at a time. The photon counter was triggered 0.5 ms before the beam pulse to monitor the PMT's dark current. A beam pulse of 1.5-ms width with a 50-ms period between pulses produced acceptable results. This corresponds to a duty cycle of 3%. A greater duty cycle may result in the electron beam heating the grain. This undesirable heating can be observed as a consistent reduction of the decay time of the emission over several consecutive measurements. Data were collected only during the first 20 ms after triggering. Since the time constant for this phosphor is about 3.2 ms at room temperature, after 20 ms there was no difference between the emitted fluorescence signal and the dark current of the PMT.

The photon counter has two channels designated by A and B. The gate settings for each channel are shown in Table 1. Channel A was operated in a gated scanning (boxcar) mode⁵ and began scanning before the electron beam was energized to include the dark current at the beginning of the cycle. Channel B was operated in the fixed mode, and counted photons from the phosphor grain at the emission peak of the electron-beam excitation pulse. For each point, a computer divided the content of channel A by the content of channel B. A complete normalized-emission decay curve was created in 100 pulses. For this experiment, the average of 10 scans was used to produce the emission curve. A typical luminescence curve for one of the grains used in the experiments is shown in Fig. 3.

Table 1. Photon-Counter Gate Settings

	Gate of Channel A	Gate of Channel B
Mode	Scanning	Fixed
Delay	0	1.8 ms
Width	400 μ s	400 μ s
Increment	200 μ s	-

The time decay for each curve is obtained by fitting data to the equation

$$Y(t) = C + A \exp-(t/t_0)$$

where $Y(t)$ is the number of photons as a function of time, C is a constant that determines the number of photons when there is no excitation (i.e., the PMT's dark current), A is the number of photons at the beginning of the curve fitting, t is time, and t_0 is the time decay and is the parameter of interest. For this experiment the curve fitting started 1 ms after the excitation pulse was turned off. This was done to obtain the most consistent results, since the decay curve is not a perfect exponential.

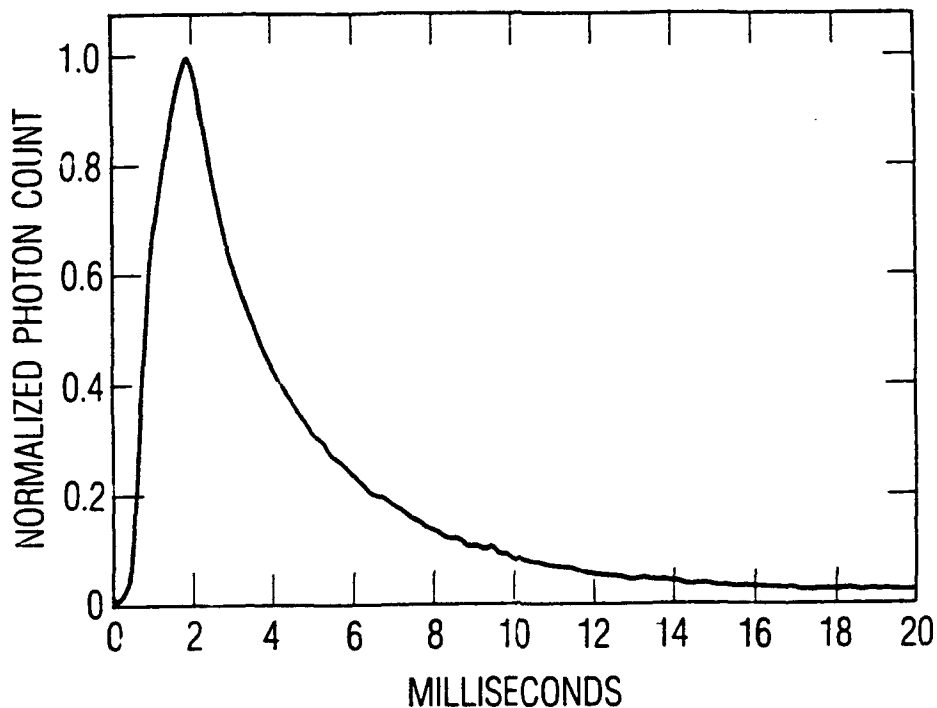


Figure 3. Typical Luminescence Curve Obtained from a MFGe:Mn Phosphor Grain

D. PROCEDURE

Once a strategically located grain was selected for temperature measurement, the SEM could be operated in either the scan or spot modes while the beam blanking was on. In the scan mode the magnification was increased and the entire grain scanned. It was found that scanning the grain over its entire area gave the most consistent results, since the luminescence is integrated over the grain's entire area. The spot mode has the potential of being useful in submicrometer measurements, since the overall diameter of the beam is less than 100 nm. For the measurements presented here, only the scan mode was used.

The first step involved calibrating selected grains by determining their time decay at room temperature. Then, power was applied to the heater embedded in the copper disk and the temperature allowed to come to equilibrium. The temperature of the copper disk was monitored with a thermocouple located near the Zener diode. It was assumed that the thermocouple reading corresponded to the temperature of the grain. The time decay for the selected grains was then remeasured. Four different time decay measurements were taken at 21, 39, 53, and 77°C, and a graph was made of the time decay versus temperature for each grain. Figure 4 shows one such graph.

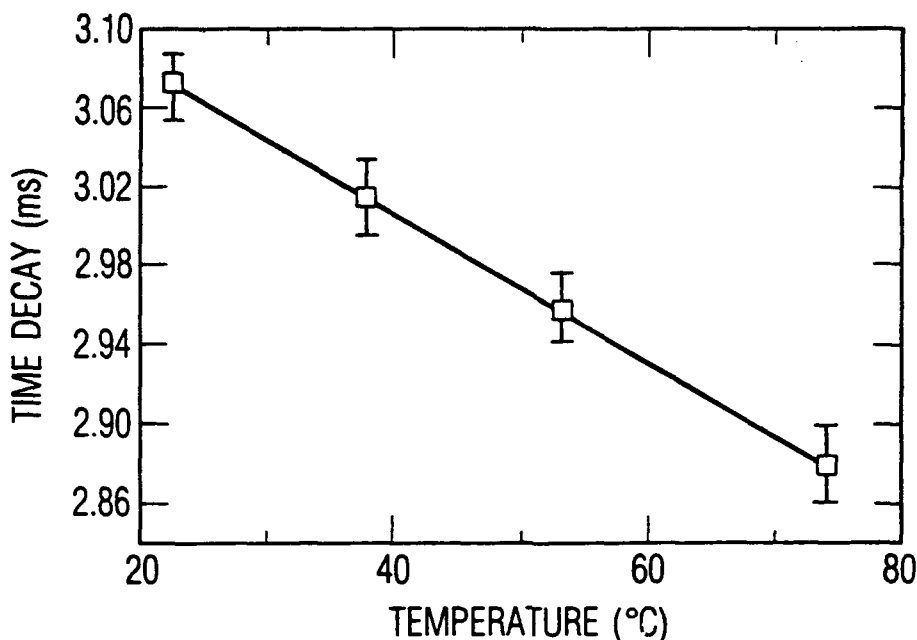


Figure 4. Time Decay vs Temperature Calibration Curve for a MFGe:Mn Phosphor Grain

The luminescence curve measurements were repeated five times, and the mean and standard deviation of the five measurements were calculated and recorded. The calibration points shown in Fig. 4 display the mean of the recorded data. For the experiment to measure true temperature, there must be a good thermal contact between the substrate and the phosphor grain. If it was noted during the calibration process that the time decay of the five measurements showed a steady decrease, the measurements were repeated five more times. If a similar behavior was observed during the second five measurements, it was concluded that there was a poor thermal contact between the grain and the substrate, and that the heating observed was caused by the e-beam. Grains exhibiting this type of behavior were disregarded.

After the grains were calibrated, the heater was turned off and reverse bias power was applied to the Zener diode by means of the dc output of the curve tracer. To reach thermal equilibrium, a bias current ($I_D = 6.5 \text{ mA}$) was applied to the diode at least 16 h before the time decay measurements started. The time decay of the grains that were calibrated was then remeasured, and the temperature of each grain was determined from its graph. Thus a thermal map of the Zener diode was obtained, as shown in Fig. 5. It was determined that the maximum temperature measured, $T \approx 133^\circ\text{C}$, approximates the actual junction temperature T_J .

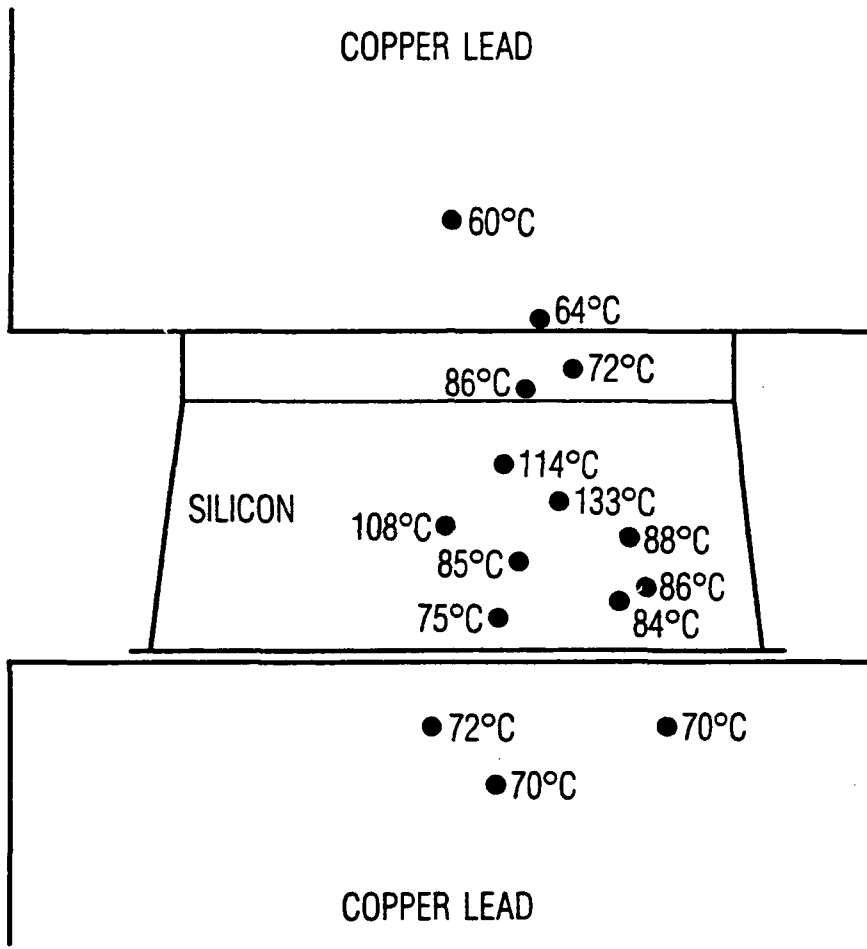


Figure 5. Thermal Map of Sectioned 22-V Zener Diode

III. RESULTS AND DISCUSSION

A. THERMAL CHARACTERISTICS OF ZENER DIODES

To confirm our experimental results, we investigated the thermal resistance of the 1N5251 plastic encapsulated, 500-mW, axial-lead, 22-V Zener diode.⁶ The power dissipation P and the junction temperature T_J are related by the equation

$$T_J = \Delta T_J + T_A = P\theta_{DL} + T_A$$

where ΔT_J is the rise in the junction temperature caused by the power dissipation, T_A is the ambient temperature, and θ_{DL} is the thermal resistance of the diode under specific operating conditions. From the manufacturer's published data, $\theta_{DL} = 250^\circ\text{C}/\text{W}$ when the diode leads are clamped to an infinite heat sink 3/8 in. from the body.⁷ In this application, an infinite heat sink was impractical. During these experiments the diode leads were attached to the thicker power leads, which acted as the heat sink. Then, the only added thermal resistance is due to the diode's own leads. Thus, the total thermal resistance of the Zener diode θ_D is

$$\theta_D = \theta_{DL} + \theta_L$$

where θ_L is the thermal resistance of the leads. θ_L can be calculated using a one-dimensional heat flow model as

$$\theta_L = \ell / (2k_{cu}\pi a^2)$$

where ℓ is the length of the lead in excess of 3/8 in. ($\ell = 1.5875$ cm), k_{cu} is the thermal conductivity of copper ($k_{cu} = 3.77$ W/cm $^\circ\text{C}$), and a is the radius of the lead ($a = 0.0254$ cm). The one-dimensional heat flow expression of the thermal resistance of a lead is divided by 2, because from the heat-generating junction boundary the heat path is equivalent to a parallel circuit. With the above numbers, θ_L can be expressed as

$$\theta_L = 103^\circ\text{C}/\text{W}$$

The total thermal resistance of the device thus becomes

$$\theta_T = 250 + 103 = 353^\circ\text{C}/\text{W}$$

The value of θ_T expressed above must be further modified. In our experiment the 1N5251 Zener diode was sectioned to expose its interior. This was accomplished by polishing off a portion of the Zener diode. As a result, the cross section of the device was reduced substantially, resulting in an increased thermal resistance. Through micrometer measurements of the body of the diode, we determined that polishing removed from 40% to 50% of the device.

Table 2. Total Thermal Resistance, Temperature Rise, and Junction Temperature for Various Segments of Zener Diode

Cross Section Removed (%)	θ_T ($^{\circ}\text{C}/\text{W}$)	$\Delta T_J = P\theta_T$ ($^{\circ}\text{C}$)	$T_J = \Delta T_J + T_A$ ($^{\circ}\text{C}$)
40	589.80	84.3	124.3
45	643.41	92.0	132.0
50	707.76	101.2	141.2

Using linear approximation, values for θ_T , ΔT_J , and T_J for a 40%, 45%, and 50% removal of the cross section of the Zener diode are shown in Table 2. This table uses a power dissipation of $P = (22 \text{ V} \times 0.0065 \text{ A}) = 0.143 \text{ W}$, and ambient temperature $T_A = 40^{\circ}\text{C}$, as measured by the thermocouple mounted on the copper heater while the Zener diode was operating. For 45% removal, the calculated ($T_J = 132^{\circ}\text{C}$) and the measured ($T_J = 133^{\circ}\text{C}$) junction temperatures are in close agreement with each other.

B. EXPERIMENTAL UNCERTAINTY

During the development of the measurement technique and also while decay time data for the Zener diode were taken, we noticed a substantial difference between two consecutive decay time measurements for a grain at a given temperature. The observed difference is in the range of $\pm 40 \mu\text{s}$ and corresponds to a temperature difference of $\pm 5^{\circ}\text{C}$.

A combination of the three sources can be responsible for the experimental uncertainty: (1) it can originate in the phosphor itself, (2) it can be the consequence of electron beam excitation, and (3) it is an experimental error inherent in the setup.

First, Wickersheim and Sun⁴ report $\pm 2^{\circ}\text{C}$ uncertainty without any calibration and $\pm 0.2^{\circ}\text{C}$ if a calibration is performed. The transient fluorescent characteristics of a phosphor are an intrinsic material property, irrespective of the method of excitation. Therefore, the first source of error does not appear significant. Only a very small percentage of the $\pm 5^{\circ}\text{C}$ uncertainty reported here appears to originate in the phosphor itself.

Second, the experimental uncertainty due to electron beam excitation consists of two major components: localized heating, and surface effects. To estimate localized heating, a Faraday cup was used at the sample location to measure sample current. A sample current, I_{sp} , of 50 pA was measured. Using an $I_{sp} = 50 \text{ pA}$, an excitation pulse of 1.5 ms, and accelerating voltage of $V = 20 \text{ kV}$, the energy per pulse is $1.5 \times 10^{-9} \text{ J}$. The rise in temperature, ΔT , per pulse can be calculated from the equation $\Delta T = Q/mc$, where Q is energy per pulse, m is mass, and c is specific heat. The specific heat of the phosphor was measured with a differential scanning calorimeter and found to be $-0.6 \text{ J/g-}^{\circ}\text{C}$. For a grain mass of about $2 \times 10^{-9} \text{ g}$, the temperature rise per pulse is 1.25°C . This calculation assumes that all the energy in the

beam is adsorbed by the grain and that the entire grain is being heated. During the experiment a single grain was scanned with the SEM's electron beam. Scanning the grain ensured that any localized heating is uniformly distributed over its entire volume. Undoubtedly, some of this heat is contributing to the uncertainty of the measurement, but with a 3% duty cycle we did not detect any systematic increase in the temperature of the grain being scanned. This would indicate that the grain has a good thermal conductivity and that the copper block is acting as a heat sink.

The interaction of the electron beam with the phosphor is limited to a shallow volume close to the surface of the grain. Because of the shallow excitation depth, it is reasonable to assume that surface effects greatly influence emission properties. A common manifestation of surface effects is a reduction in the lifetime of carriers; this results in a measured time constant that is somewhat less than the actual time constant at the given temperature. In support of this hypothesis, it should be noted that when the energy of the electron beam was increased, not only did the photon count increase (due to the greater excitation volume), but the measured time constant also increased. An increase of about 5 keV in beam energy corresponded to an increase of greater than 300 μs in the measured time constant. Also, since the thickness of the adhesive film coating varies along the surface of the grain, the excitation volume depends on the position of the beam, so that the contribution of surface effects to the measured time-decay constant depends on the spot where the excitation occurs. This explains (1) variations in the time decay and photon count in the case of spot-mode excitation of a single grain, and (2) why it was necessary to find the same spot in this mode to obtain repeatable results.

During the experiment we selected grains that exhibited good thermal contact to the substrate, and a single grain was scanned at a time. Thus, we tried to minimize the effects of localized heating. With the present experimental arrangement, it is not possible to separate the source of error to determine its relative contribution. This could be the subject of a future study. We believe that the electron beam excitation of the phosphor grain can be the source of the observed uncertainty, with the surface effects contributing the greater portion.

Third, the method of time decay measurement itself introduces an experimental error. All counters have a limit when trying to resolve two consecutive pulses; this limit is usually expressed as the maximum count rate for pulses arriving at regular intervals, or as the minimum pulse-pair resolution limit for pulses arriving randomly. For random events, a counter may miss a count when two pulses arrive within a time interval that is less than the pulse-pair resolution limit. The probability that a photon is counted is equal to the probability that no photon arrived during the time t preceding the event, where t is the pulse-pair resolution limit of the counter. If we let K define the total average photon count-rate per second, then the probability that each photon is detected is $\exp(-Kt)$. As Kt increases, the detection probability decreases and photon pulses may be lost. Calculations show that, with our count rate of about 2000 photons per pulse period, practically all photons that cause a current pulse are counted.

We have listed several possibilities for measurement error. While we are unable to pinpoint the source of our experimental error, we report a $\pm 5\%$ measurement accuracy.

IV. CONCLUSIONS

A technique has been developed for measuring temperatures with a spatial resolution less than 10 μm . This task is accomplished by measuring, with the aid of a photomultiplier tube and a photon counter, the time decay fluorescence of an inorganic phosphor. The phosphor used is magnesium fluorogermanate activated with manganese. This compound exhibits a temperature-dependent fluorescence that decreases monotonically with temperature. The spatial resolution is obtained by illuminating, with an electron beam, individual phosphor grains.

The junction temperature of a plastic encapsulated, 500-mW, axial-lead, cross-sectioned, 22-V Zener diode was measured with this technique. The measured temperature and the predicted junction temperature from the manufacturer's specifications are in close agreement. The uncertainty of the temperature measurement is less than $\pm 5^\circ\text{C}$.

One important aspect of our work is the verification of existing thermal models of semiconductor devices. This verification is obviously most important for microwave and power devices, whose expected length of reliable operation is a function of actual junction temperature.

REFERENCES

1. C. C. Williams and H. K. Wickramasinghe, "Scanning thermal profiler," *Appl. Phys. Lett.* **49** (23) 1587-1589 (8 December 1986).
2. P. Kolodner and J. A. Tyson, *Appl. Phys. Lett.* **40**, 782 (1982); P. Kolodner and J. A. Tyson, *Appl. Phys. Lett.* **42**, 117 (1983).
3. K. A. Wickersheim and M. H. Sun, "Fiberoptic Thermometry and its Applications," *J. Microwave Power*, 85-94 (1987).
4. K. A. Wickersheim and M. H. Sun, "Fluoroptic Thermometry," *Medical Electronics*, 84-91 (February 1987).
5. Stanford Research Systems, Inc., Application Note, *Signal Recovery with Photomultiplier Tubes Using Photon Counting, Lock-in Detection, and Boxcar Averaging*.
6. Motorola Inc., *The Semiconductor Data Library*, 1st ed., Vol. 2 (1972).
7. Microsemi Corp., *Microsemi Data Book* (1987-1988).

TECHNOLOGY OPERATIONS

The Aerospace Corporation functions as an "architect-engineer" for national security programs, specializing in advanced military space systems. The Corporation's Technology Operations supports the effective and timely development and operation of national security systems through scientific research and the application of advanced technology. Vital to the success of the Corporation is the technical staff's wide-ranging expertise and its ability to stay abreast of new technological developments and program support issues associated with rapidly evolving space systems. Contributing capabilities are provided by these individual Technology Centers:

Electronics Technology Center: Microelectronics, solid-state device physics, VLSI reliability, compound semiconductors, radiation hardening, data storage technologies, infrared detector devices and testing; electro-optics, quantum electronics, solid-state lasers, optical propagation and communications; cw and pulsed chemical laser development, optical resonators, beam control, atmospheric propagation, and laser effects and countermeasures; atomic frequency standards, applied laser spectroscopy, laser chemistry, laser optoelectronics, phase conjugation and coherent imaging, solar cell physics, battery electrochemistry, battery testing and evaluation.

Mechanics and Materials Technology Center: Evaluation and characterization of new materials: metals, alloys, ceramics, polymers and their composites, and new forms of carbon; development and analysis of thin films and deposition techniques; nondestructive evaluation, component failure analysis and reliability; fracture mechanics and stress corrosion; development and evaluation of hardened components; analysis and evaluation of materials at cryogenic and elevated temperatures; launch vehicle and reentry fluid mechanics, heat transfer and flight dynamics; chemical and electric propulsion; spacecraft structural mechanics, spacecraft survivability and vulnerability assessment; contamination, thermal and structural control; high temperature thermomechanics, gas kinetics and radiation; lubrication and surface phenomena.

Space and Environment Technology Center: Magnetospheric, auroral and cosmic ray physics, wave-particle interactions, magnetospheric plasma waves; atmospheric and ionospheric physics, density and composition of the upper atmosphere, remote sensing using atmospheric radiation; solar physics, infrared astronomy, infrared signature analysis; effects of solar activity, magnetic storms and nuclear explosions on the earth's atmosphere, ionosphere and magnetosphere; effects of electromagnetic and particulate radiations on space systems; space instrumentation; propellant chemistry, chemical dynamics, environmental chemistry, trace detection; atmospheric chemical reactions, atmospheric optics, light scattering, state-specific chemical reactions and radiative signatures of missile plumes, and sensor out-of-field-of-view rejection.